Article

Cellular Uptake of Gold Nanoparticles and Their Behavior as Labels for Localization Microscopy

Felipe Moser,[1] Georg Hildenbrand,[1,2] Patrick Müller,[1] Alexander Al Saroori,[1] Abin Biswas,[1,2] Margund Bach,[1] Frederik Wenz,[2] Christoph Cremer,[3,4] Nina Burger,[2] Marlon R. Veldwijk,[2] and Michael Hausmann[1,*]

[1]Kirchhoff-Institute for Physics, Faculty of Physics and Astronomy and [2]Department of Radiation Oncology, Medical Faculty Mannheim, Universitätsmedizin Mannheim; [3]Institute of Pharmacy and Molecular Biotechnology, Heidelberg University, Heidelberg, Germany; and [4]Institute of Molecular Biology, Mainz, Germany

ABSTRACT Gold nanoparticles (GNPs) enhance the damaging absorbance effects of high-energy photons in radiation therapy by increasing the emission of Auger-photoelectrons in the nm-μm range. It has been shown that the incorporation of GNPs has a significant effect on radiosensitivity of cells and their dose-dependent clonogenic survival. One major characteristic of GNPs is also their diameter-dependent cellular uptake and retention. In this article, we show by means of an established embodiment of localization microscopy, spectral position determination microscopy (SPDM), that imaging with nanometer resolution and systematic counting of GNPs becomes feasible, because optical absorption and plasmon resonance effects result in optical blinking of GNPs at a size-dependent wavelength. To quantify cellular uptake and retention or release, SPDM with GNPs that have diameters of 10 and 25 nm was performed after 2 h and after 18 h. The uptake of the GNPs in HeLa cells was either achieved via incubation or transfection via DNA labeling. On average, the uptake by incubation after 2 h was approximately double for 10 nm GNPs as compared to 25 nm GNPs. In contrast, the uptake of 25 nm GNPs by transfection was approximately four times higher after 2 h. The spectral characteristics of the fluorescence of the GNPs seem to be environment-dependent. In contrast to fluorescent dyes that show blinking characteristics due to reversible photobleaching, the blinking of GNPs seems to be stable for long periods of time, and this facilitates their use as an appropriate dye analog for SPDM imaging.

INTRODUCTION

Radiotherapy is a fundamental part of cancer treatment (1). The radiation dose given to the tumor is, among other constraints, strongly limited by the conditions surpassing damaging of the surrounding normal tissue. Novel radiation technologies, treatment planning, and treatment delivery have resulted in increased sparing of normal tissue outside the clinical target volume, thus leading to an increased therapeutic gain (2). Nevertheless, normal-tissue reactions from high doses delivered to the tumor target are still a major concern. Methods of broadening the therapeutic gain are still required along with investigations that result in an increased radiosensitivity and radiation susceptibility of the tumor while keeping normal tissue at normal radiosensitivity.

One possibility for enhancing the radiosensitivity of tumor cells is the tumor-specific incorporation of materials (nanoparticles, nanorods) with a high atomic number (high-Z) (3). The higher the atomic number, the higher the probability of photon interactions by the photoelectric effect. Induced photoelectrons are of high energy and long-ranged (up to several 100 μm in water), and primarily deposit their energy further from the originating source along the photon interaction path. Generated Auger electrons, on the other hand, have lower energy and therefore a shorter range (<1 μm), leading to short-ranged dose enhancement (4,5).

Using intravenously injected gold ($Z = 79$) nanoparticles (GNPs) of 1.9 nm diameter as radiosensitizers, Hainfeld et al. (6) showed a significant increase in one-year survival (20% for x-rays alone versus 50–86% for x-rays with GNPs) of mice with tumors treated with 250-kV x-ray energy. This pioneering work has been further developed in different tumors and applications (7–9). Accumulation of GNPs in the tumor tissue was achieved by passive targeting. Particles larger than 300 nm are potentially eliminated by macrophages; smaller particles, typically between 10 and 100 nm diameter, can enter the tumor tissue (10). Experiments showed dose enhancement factors of 1.17–1.66 (11–13), depending on the x-ray energy applied. The optimum size of GNPs for cellular uptake and retention was found to be 50 nm (3,14). GNPs smaller than 30 nm are leaving the cell again by passive diffusion (15). The requirement of very small particles for an enhanced radiosensitivity appears to thus be contrary to the optimum diameter for cellular uptake.

To overcome these limitations, we have recently shown that 10 nm particles may be a feasible compromise. To our knowledge, a new method aimed at enhancing cellular uptake efficiency and retention of smaller GNPs was

Submitted October 15, 2015, and accepted for publication January 4, 2016.

*Correspondence: hausmann@kip.uni-heidelberg.de

Felipe Moser and Georg Hildenbrand contributed equally to this work.

Editor: Paul Wiseman.

0006-3495/16/02/0947/7

http://dx.doi.org/10.1016/j.bpj.2016.01.004

developed. A quantity of 10 nm GNPs was linked to a PCR product that was generated with a thiol group in the 5′ primer. The GNP-DNA complex was then transferred into the tumor cells by transient transfection (henceforth, such experiments shall be called "GNP transfection" experiments). To determine the uptake efficiency, localization microscopy was performed and the relative count rates were measured. Increased radiosensitization was shown for this method on HeLa cells by determining the clonogenic survival rates after irradiation with 6-MV x-rays (16).

Until now, mostly size-dependent correlations of GNP uptake have been studied. Quantification of absolute values of uptaken GNP numbers has been almost neglected due to the complexity of the required preparation and measurement by electron microscopy (10). For instance, mechanically prepared slices in the order of 100 nm were not compatible with the conservation of an intact three-dimensional (3D) cell morphology. Because GNPs are able to support radiotherapy, there has been a growing interest in methods that allow for the quantifications of GNP shape and size in 3D-conserved cells. In this article, localization microscopy studies (17) are presented that quantify passive cellular uptake and retention/release of 10 nm and 25 nm GNPs after incubation, as well as 25 nm GNP-DNA after transfection. Special focus will be drawn on the optical behavior of GNPs.

It has been shown that GNPs or particles with a gold shell are fluorescent at different absorption and emission wavelengths, a characteristic dependent on the particle diameter or the shell thickness, respectively (18). Size-dependent color (Tyndall color) could be due to Mie scattering (19). GNPs can cover the entire optical spectrum from UV over visible wavelengths to near-infrared for which the application of GNPs as hyperthermic reagents was demonstrated (20). Moreover, luminescent blinking was found for GNPs approximately one decade ago (21). This behavior makes them interesting for spectral position determination microscopy (SPDM), a special embodiment of localization microscopy (22,23). SPDM normally discriminates individual dye molecules or fluorescent particles by stochastic switching of their fluorescence between off- and on-stages over a particular lifetime. Taking a time series of images registering these blinking effects allows precise determination (nm precision) of the spatial position of the blinking molecule/particle. Distances in the 10 nm range can be resolved between two molecules/particles and calculated with nanometer precision (24).

MATERIALS AND METHODS

Cell culture and GNP incorporation

For the experiments, HeLa cells (obtained from the Tumor Cell Bank of the German Cancer Research Center, Heidelberg, Germany) were used. The cells were cultured in DMEM with $NaHCO_3$, D-glucose, stable glutamine, and Na-pyruvate, with 10% fetal bovine serum, 1% HEPES buffer, and 1% penicillin-streptomycin.

To prepare the cells for GNP transfection (25 nm Aurion Gold Sols; Aurion, Wageningen, The Netherlands), the cells were cultured on sterile circular 10 mm coverslips. Each coverslip was allowed to grow over with 15,000–20,000 cells, so that cell clumping was prevented. This corresponded with 70–80% confluent growth, so that it was easier to image single cells by SPDM. According to Burger et al. (16), the transfection was performed with DNA-modified GNP (GNP-DNA).

For pure GNP incubation, cells were cultured on square 24-mm coverslips. The incubation was performed by replacing the cell-culture medium with a solution of culture medium and Aurion Gold Sols (25 and 10 nm) for 2 and 18 h. The particle concentration was 0.2 nM, unless otherwise stated.

For microscopy, the cells were finally fixed in 4% formaldehyde freshly prepared from paraformaldehyde and embedded into ProLong Gold antifade mounting medium (2 μL for the 10 mm circular coverslips and 15 μL for the 24 $\times$ 24 mm coverslips; Thermo Fisher Scientific, Waltham, MA) and stored at 4°C until use. The fixation and embedding procedure ensured that the 3D shape of the cells could be well maintained.

SPDM imaging

Localization microscopy (SPDM) was done with illumination at two wavelengths using two diode-pumped, solid-state lasers with illumination intensity maxima at 491 and 561 nm and 200 mW power. The instrument was equipped with an oil objective lens 63×/NA 0.7…1.4 (Leica, Wetzlar, Germany) and an electron-multiplying charge-coupled device camera (1376 × 1040 pixels; Andor Technology, South Windsor, CT). The images were acquired via band-pass filters (525/50 nm for 491 nm excitation and 609/54 nm for 561 nm excitation).

Specimen sections with cell monolayers were considered for SPDM imaging. The cells were selected visually. Special care was taken that the cells were individualized and overlapping to other cells circumvented. An optical section of 600 nm depth was acquired from which time stacks of typically 2000 frames were acquired at an integration time of 55 ms each. To get comparable conditions, the cell nuclei were selected in such a way that the image section was taken at the largest diameter.

For quantitative image evaluation, in-house programs were applied. The loci matrix was produced by a maximum-likelihood-based algorithm with a possibility to subtract background (25). This program reduce the acquired time stack of images to an artificial image of the cell nucleus overlaid by the matrix of the spatial positions of the intensity maxima recorded from the blinking GNPs. Based on these images, counting of particles in the given image section was performed. Further evaluation programs based on MATLAB (The MathWorks, Natick, MA) were used for the calculation of the localization precision or other image parameters (for further details, see Kaufmann et al. (24), Müller et al. (26), and Stuhlmüller et al. (27)). Because it has already been shown that the detection procedure and software was sensitive enough to separate signals in the dimensions of the applied particles (27), effects of overlapping signals were mostly negligible. In addition, (damaged) cells indicating the formation of big aggregates leading to nonfluorescent, absorbing clumps (appearing as black regions in the images within a GNP environment) were excluded from quantitative evaluation.

For comparison of particle numbers in different experiments, a two sample *t*-test (Welch test) (28) was applied. In addition to the number of particles, the localization precision of the particle signals was determined.

Absorption measurements

For the absorption measurements, GNPs of 10 and 25 nm diameter were diluted in sodium-phosphate buffer stabilized by *Streptomyces avidinii* proteins and 0.05% sodium acid. For comparison, the absorption spectra of HeLa cells carrying the respective GNPs were also measured.

RESULTS

Quantities of 10 and 25 nm GNPs were incorporated into HeLa cells by incubation (10 nm, 25 nm GNPs) or transfection (25 nm GNP-DNAs). After 2 h, a significant incorporation was visible, although no clustering of GNPs was observed. The cells were intact and did not show any obvious alterations as determined by systematic visual inspection (see, for example, Fig. 1). After 18 h, however, the GNPs tended to form clusters that were visible, and also formed fluorescent aggregates when imaged via SPDM (for example, see Fig. 2). For the transfected 25-nm GNPs, the clusters were smaller, but appeared to be more frequently distributed over the whole cytoplasm in comparison to the incubation experiments (for example, Fig. 2 versus Fig. 4).

To quantify and compare the results, SPDM measurements were performed and the absolute numbers of 10 and 25 nm GNPs were determined in randomly selected cells of the specimens. The GNPs were excited at 561 nm as a wavelength fitting ~2/3 of the absorption intensity maximum of the used particles (Fig. 3). In addition, the average localization precision (precision of determination of the intensity barycenter) was determined for each cell to parameterize the quality of the acquired image stacks. Because the localization precision is dependent on the signal/background noise, it represents a measure for specimen quality and has a strong impact on the comparability of images and results.

In Table 1, the results of particle frequency and localization precision are summarized for the 10 nm GNPs incubated at a concentration of 0.2 nM. According to the applied *t*-test, no significant difference was obtained between 2 and 18 h incubation. On average, a slight increase of the localization precision was found after 18 h incubation with a considerable reduction of the variation. Additionally, other concentrations of GNPs were applied (2 and 5 nM), but did not result in improved uptake or cell conservation (data not shown).

In contrast, 25 nm GNPs showed a significant increase (~15-fold) of the particle amount after 18 h incubation in comparison to 2 h incubation (Table 2). The localization precision was nearly constant for the low concentration after 2 h, whereas much higher variations were observed after 18 h, indicating increased cellular activity.

The incubation experiments for 25 nm GNPs were compared to results obtained after transfection experiments with the similar-sized particles. In the latter case, according to the *t*-test, no significant difference was obtained for the amount of particles observed between 2 and 18 h treatment (Table 3). Again, an improved localization precision was measured after 18 h.

To prove whether the measured SPDM signals at 561 nm are due to the GNPs and not dependent upon label-free fluorescence/autofluorescence of biological molecules (for comparison, see Gossett (28)), the 25 nm GNP experiments after 2 h transfection were subjected to two-wavelength illumination (491 nm, 561 nm). The illumination at 491 nm is already known to activate label-free biomolecules and to cause blinking in SPDM measurements (29). In Fig. 4, an example of a cell is shown. The signals excited at 491 nm (shown in *red*) do not appear to colocalize with the signals excited at 561 nm (shown in *green*), indicating that both types of signals may be of different origin. The results (Table 4) indicate the same localization precision for both wavelengths. The amount of detected signals, however, was significantly (according to the applied *t*-test) higher by approximately a factor of 2 at 491 nm in comparison to 561 nm.

In Table 5, the averaged data of all conducted experiments are summarized. Uptake of incubated GNPs seems to be a natural behavior of HeLa cells so that after 2 h a considerable amount of both types of GNPs has always been registered. However, a clear size-dependent difference was observed. Whereas for 10 nm GNPs an increment of particles at 2 h and a decrement of particles at 18 h were found, the amount of 25 nm GNPs was further increasing at 18 h. This may indicate a better uptake and retention of

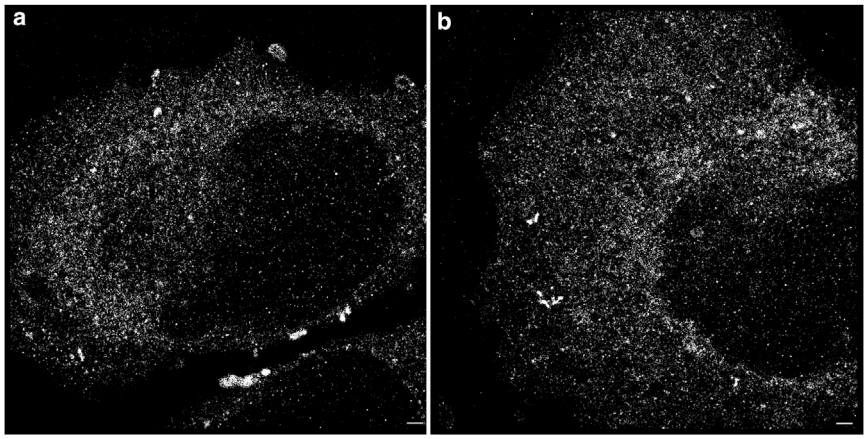

FIGURE 1 (*a* and *b*) Two examples of SPDM images of HeLa cells subjected to transfection (2 h) of GNP-DNAs that have an average diameter of 25 nm. The cells were illuminated at 561 nm. Each point represents a GNP arranged in the cytoplasm. The pointilistic pattern results from a time stack of images in which the loci of the individual blinking events were represented by a point. Scale bar, 500 nm.

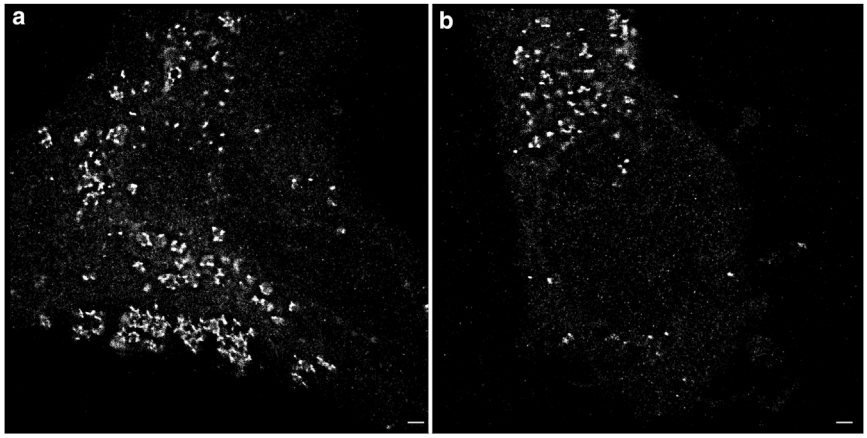

FIGURE 2 (*a* and *b*) Two examples of SPDM images of HeLa cells subjected to transfection (18 h) of GNP-DNAs that have an average diameter of 25 nm. The cells were illuminated at 561 nm. Each point represents a GNP arranged around the cell nucleus in the cytoplasm. Compared to Fig. 1, the pointilistic pattern (obtained from a time stack of images in which the loci of the individual blinking events are represented by a point) shows visible clustering. Scale bar, 500 nm.

25 nm GNPs in comparison to 10 nm GNPs. Although the absolute amount of 25 nm GNP-DNA was considerably higher after transfection of 2 h, a further increase of particle uptake was found in transfection experiments after 18 h, too. The absolute amount of GNP uptake was also found in the two-color experiment, indicating that the signals excited at 491 nm are not due to GNPs.

DISCUSSION

The application of GNP to enhance cell damaging effects in radiotherapy has been studied in multiple cell culture and animal experiments (for review, see Ngwa et al. (3) and Chithrani and Chan (14)). Until now, mostly size-dependent correlations of GNP uptake have been studied and optimized. Quantification of absolute values of uptaken GNP numbers was almost neglected due to the complexity of the required preparation and measurement by electron microscopy (10). Because systematic studies of size- and shape-dependent amounts of GNPs are supportive for research and clinical studies and thus for radio-therapy, easy-to-handle techniques for GNP quantification in 3D-conserved cells are required. Here, we present the application of SPDM (17,22,23), an embodiment of localization microscopy, as such an alternative method. SPDM has the advantage of providing superresolution in the nanometer regime comparable to that of electron microscopy, while using established preparation techniques for light microscopy (23) and commercially available optics and detection devices. Our results show the feasibility of SPDM for GNP quantification on a single-cell basis and are supported by electron microscopy experiments described in Chithrani

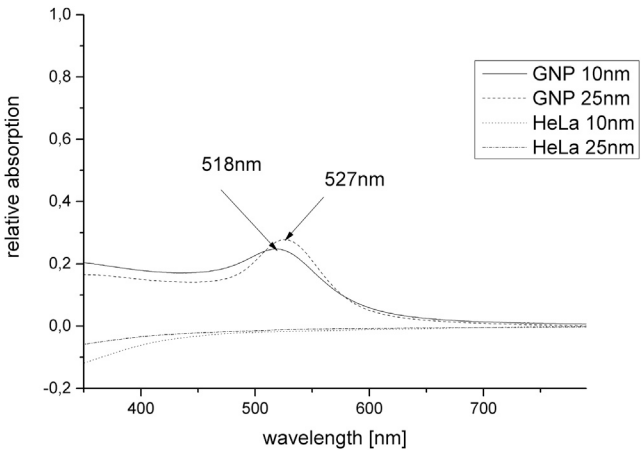

FIGURE 3 Absorption spectra of the applied GNPs in solution. The maxima of the plasmon resonance peaks were detected at 518 nm (10 nm GNPs) and 527 nm (25 nm GNPs). For comparison, the HeLa cells did not show any relevant absorption.

TABLE 1 Numbers of Counted Points and Average Localization Precision per Image: 10 nm GNPs

Cell Number	Counts of GNP Points (2 h)	Counts of GNP Points (18 h)	Localization Precision (2 h) (nm)	Localization Precision (18 h) (nm)
1	1230	12,498	14.44	20.73
2	28,245	14,379	18.87	21.27
3	13,649	13,711	19.32	21.07
4	1762	6150	5.87	22.25
5	25,055	9699	19.03	22.27
6	14,754	8519	20.00	22.12
7	11,877	8995	20.38	21.52
8	12,563	8118	20.86	22.33
9	14,414	3597	18.79	21.53
10	7285	12,703	19.80	21.84
11	1438	10,362	17.57	21.61
12	4491	8658	34.94[a]	20.22
13	4262	8242	35.83[a]	21.75
14	20,404	9374	31.67[a]	22.51
15	7632	5908	33.53[a]	20.97
Average	11,271	9394	17.20	21.60
SD	8466	2998	8.33	0.66
Error of the mean	2263	801	2.23	0.18

The GNPs were incubated for 2 and 18 h and illuminated at 561 nm.
[a]Obtained with a slightly differently positioned localization detection lens. This resulted in a lower amount of signals, so the threshold of the analysis was adjusted. This means that the amount of counted points is consistent with the rest of the measurements, but the localization precision was poorly affected.

TABLE 2 Numbers of Counted Points and Average Localization Precision per Image: 25 nm GNPs

Cell Number	Counts of GNP Points (2 h)	Counts of GNP Points (18 h)	Localization Precision (2 h) (nm)	Localization Precision (18 h) (nm)
1	8889	132,407	35.41	29.08
2	7080	87,947	34.93	28.33
3	5643	80,033	35.48	27.77
4	5319	129,931	34.33	29.26
5	5674	86,264	35.10	28.51
6	4447	89,280	34.91	27.02
7	8312	75,994	35.18	28.96
8	3725	64,416	35.21	30.55
9	6644	85,708	35.22	26.38
10	3557	75,241	35.41	28.64
11	4385	99,061	35.45	13.10[a]
12	4816	113,125	34.38	14.96[a]
13	7166	88,753	33.83	16.10[a]
14	8508	118,022	35.72	15.64[a]
Average	5790	91,829	35.01	24.25
SD	1575	17,888	0.52	6.31
Error of the mean	437	4961	0.14	1.75

The GNPs were incubated for 2 and 18 h and illuminated at 561 nm.
[a]Obtained with a slightly differently positioned localization detection lens. This resulted in a lower amount of signals, so the threshold of the analysis was adjusted. This means that the amount of counted points is consistent with the rest of the measurements, but the localization precision was poorly affected.

et al. (10) and other biological results obtained by bulk experiments (see, for instance, Chithrani et al. (10) and Burger et al. (16)).

TABLE 3 Numbers of Counted Points and Average Localization Precision per Image: 25 nm GNP-DNAs

Cell Number	Counts of GNP Points (2 h)	Counts of GNP Points (18 h)	Localization Precision (2 h) (nm)	Localization Precision (18 h) (nm)
1	34,322	177,317	22.96	13.37
2	40,256	77,183	19.94	13.61
3	29,247	21,647	22.56	18.94
4	48,221	135,444	21.71	16.34
5	56,632	35,463	22.43	16.79
6	29,461	78,755	23.04	18.16
7	33,216	40,648	22.83	18.03
8	41,670	35,162	21.98	22.88
9	24,999	61,894	22.92	18.40
10	30,571	80,227	22.62	15.53
11	56,202	71,919	22.04	19.54
12	49,678	68,149	22.32	15.78
13	37,760	31,384	17.11	18.39
14	39,948	63,800	22.48	16.33
15	55,365	53,300	21.29	15.74
16	76,293	37,815	20.60	20.01
17	40,858	21,952	19.77	17.64
18	76,407	62,214	19.90	13.34
19	59,985	86,939	21.12	16.34
20	54,478	48,333	19.84	18.85
21	70,317	48,246	20.26	20.71
22	69,337	69,800	17.84	16.62
Average	47,965	63,981	21.25	17.33
SD	15,736	36,094	1.67	2.39
Error of the mean	3434	7876	0.36	0.52

The GNPs were transfected for 2 and 18 h and illuminated at 561 nm.

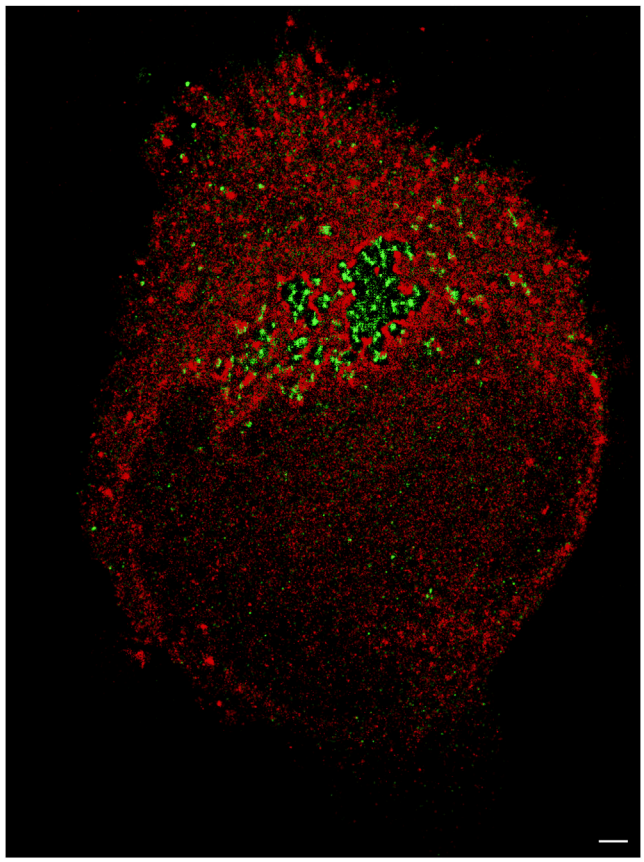

FIGURE 4 Overlay of SPDM images of a HeLa cell (incubated with 0.2 nM GNP of 25 nm) subjected to 491 and 561 nm illumination. To compare this image to Figs. 1, 2, and 3, the fluorescent points excited at 561 nm are shown in green; red points present the fluorescent blinking events detected after excitation at 491 nm. Scale bar, 500 nm. To see this figure in color, go online.

There is clearly strong evidence to suggest plasmon resonance effects (30) of the 10 and 25 nm GNP particles present a blinking in the cytoplasm when the GNPs are excited with a 200 mW laser beam. This makes them potential candidates to use as dyes in localization microscopy (17). Because the blinking effect (21) is not based on reversible photobleaching but on plasmon resonance effects, GNP labeling may be a stable tag for any future specific labeling strategies and help to circumvent existing shortcomings of conventional blinking dyes that can go into a permanently bleached state during SPDM measurements. Systematic studies of this nonbleaching behavior (18) are so far missing, especially for SPDM imaging. This topic is under investigation, and will be presented elsewhere. Here, the focus has been drawn to the GNP uptake and its correlation with SPDM imaging outcomes to obtain a feasible method for biomedical studies.

All HeLa cells showed blinking of GNPs throughout the cytoplasm and maintained the GNP incorporation at least for short periods of time without any external biochemical or physical support. It is evident that the uptake is very strongly dependent on the size of the particle, supporting

TABLE 4 Numbers of Counted Points and Average Localization Precision per Image: 25 nm GNP-DNAs

Cell Number	Counts of Points (@ 491 nm)	Counts of Points (@ 561 nm)	Localization Precision (@ 491 nm) (nm)	Localization Precision (@ 561 nm) (nm)
1	137,865	34,322	20.88	22.96
2	148,376	40,256	20.70	19.94
3	58,668	29,247	21.27	22.56
4	38,382	48,221	21.86	21.71
5	84,829	56,632	21.21	22.43
6	116,073	29,461	21.36	23.04
7	131,075	33,216	21.79	22.83
8	67,991	41,670	21.52	21.98
9	62,401	24,999	22.06	22.92
10	36,086	30,571	21.64	22.62
11	36,518	56,202	20.90	22.04
12	94,987	49,678	20.91	22.32
13	60,775	37,760	21.82	17.11
14	58,279	39,948	21.20	22.48
15	88,103	55,365	21.69	21.29
Average	81,361	40,503	21.38	21.88
SD	37,341	10,554	0.42	1.54
Error of the mean	9980	2821	0.11	0.41

The GNPs were transfected for 2 h. The cells were illuminated at 491 and 561 nm.

electron microscopic results described in Chithrani et al. (10). It is understood that nanoparticles of up to 30 nm in diameter can be incorporated through endocytosis but either the process itself is different for 10 nm and 25 nm particles, or the size of the particle results in a slower realization of the same process. In the case of 2 h of incubation, the 10 nm particles show ~90% more signals than their 25 nm counterparts. After 18 h of incubation, however, the situation is reversed. The 25 nm particles present an ~15-fold increase in signals, which is approximately a factor-of-10 higher than for the 10 nm GNPs. The maximum uptake time in the case of the 10 nm particles is closer to 2 h, while for the 25 nm particles it is closer to 18 h. Thus it appears that 25 nm particles are internalized with slower kinetics than 10 nm particles, but accumulate in higher concentrations due to a better retention (16). In addition, proceeded exclusion of 10 nm particles might occur after 18 h. Such differences have to be considered if GNPs are injected into tumor tissues for further radiotherapy.

In contrast, 25 nm GNP-DNAs also showed a strong increase of particles after 2 h, which seem to be relatively stable (within the measured errors) until 18 h. This increased incorporation kinetics may be due to the transfection reagent as Burger et al. (16) have shown by using unmodified GNPs with the transfection reagent. Overall, the transfection experiments confirmed the results obtained by Burger et al. (16) as being the most effective, with respect to the accumulated number of particles.

The average amount of points measured for the same cells (25 nm GNP-DNA transfected after 2 h of incubation) at two different wavelengths (excitation at 561 and 491 nm) indicates that GNP blinking could be separated from label-free blinking of biological molecules sui generis of the cells as it has been demonstrated by Kaufmann et al. (29).

This may, however, offer the opportunity to suppress the internal signals by SPDM because it is expected that, after high-power illumination, a considerable bleaching will take place that may be circumvented if GNPs are used as labeling tags.

In conclusion, the results indicate that GNPs in combination with SPDM may offer several, to our knowledge, novel technological aspects. On the one hand, GNPs of different sizes could be applied as labeling tags with slightly spectrally shifted fluorescence signals. For example, classical GNP-labeled antibodies could be used in combination with SPDM as a selective nonbleachable marker. On the other hand, the quantification by means of SPDM could in general support the application in many fields of research and treatment, especially in radiotherapy as, for instance, by an estimate of appropriate GNP concentrations in different types of tumor cells for assisting in optimizing the damage generated by irradiation processes. Moreover, precise visualization of the GNP positions in cells will allow experimental quantification of GNPs around short-range accessible, sensitive damage sites and targets. This will potentially open new perspectives in research where GNP constructs are used to improve the overall therapeutic gain by increasing the damage induced on specific intracellular targets (2).

AUTHOR CONTRIBUTIONS

F.M. performed measurements and evaluated data; G.H. designed research, analyzed data, and wrote parts of the article; P.M. contributed cell culture tools and preparation techniques; A.A.S. supported the measurements; A.B. supported the research; M.B. performed measurements; F.W. contributed treatment tools; C.C. contributed microscopic tools; N.B. supported

TABLE 5 Overview of the Averaged Results of Tables 1, 2, 3, and 4

Method	Average Number of Points ± SD (2 h)	Average Number of Points ± SD (18 h)	Changes between the Number of Points (from 2 to 18 h) (%)
Incubation 10 nm @ 561 nm (Table 1)	11,271 (±8466)	9394 (±2998)	−17
Incubation 25 nm @ 561 nm (Table 2)	6012 (±1780)	90,869 (±25,093)	+1411
Transfection 25 nm @ 561 nm (Table 3)	47,965 (±15,736)	63,981 (±36,094)	+33
Transfection 25 nm @ 561 nm (Table 4)	40,503 (±10,554)	not measured	—
Transfection 25 nm @ 491 nm (Table 4)	81,361 (±37,341)	not measured	—

research; M.R.V. supported research and contributed laboratory tools; and M.H. supervised F.M. and A.A.S., and prepared the final article.

ACKNOWLEDGMENTS

The authors thank Professor Dr. Dieter P. Herten, Bioquant Heidelberg for the access to the spectrometer. The authors also thank Dr. Corina-Cornelia Seegler-Sandbanck (European Institute of Feasibility Studies, Strasburg) for finding a way to clarify the subject.

M.H. gratefully acknowledges the financial support of the German Federal Ministry for the Environment, Nature Conservation, Building and Nuclear Safety (FKZ: SR/StSch/INT No. 3610S30015). Data curation and archiving has been supported (to M.H.) by the Helmholtz Portfolio Extension Large Scale Data Management and Analysis with contributions from the Data Life Cycle Lab Key Technologies and the Data Services Integration Team. Furthermore, the support of the Innovation Fond "Frontier" of the Heidelberg University within the excellence initiative of the Deutsche Forschungsgemeinschaft (to G.H. and M.H.) is gratefully acknowledged.

REFERENCES

1. Boyle, P., and B. Levin. 2008. World Cancer Report 2008. International Agency for Research on Cancer, Lyon, France.
2. Wenz, F., U. Tiefenbacher, …, K. J. Weber. 2001. Auf der suche nach der *Therapeutischen Breite* in der radioonkologie. *Onkologie.* 24 (*Suppl 5*): 51–55.
3. Ngwa, W., R. Kumar, …, G. M. Makrigiorgos. 2014. Targeted radiotherapy with gold nanoparticles: current status and future perspectives. *Nanomedicine (Lond.).* 9:1063–1082.
4. Hossain, M., and M. Su. 2012. Nanoparticle location and material dependent dose enhancement in x-ray radiation therapy. *J. Phys. Chem. C Nanomater. Interfaces.* 116:23047–23052.
5. Zygmanski, P., B. Liu, …, E. Sajo. 2013. Dependence of Monte Carlo microdosimetric computations on the simulation geometry of gold nanoparticles. *Phys. Med. Biol.* 58:7961–7977.
6. Hainfeld, J. F., D. N. Slatkin, and H. M. Smilowitz. 2004. The use of gold nanoparticles to enhance radiotherapy in mice. *Phys. Med. Biol.* 49:N309–N315.
7. Hainfeld, J. F., F. A. Dilmanian, …, H. M. Smilowitz. 2008. Radiotherapy enhancement with gold nanoparticles. *J. Pharm. Pharmacol.* 60:977–985.
8. Hainfeld, J. F., F. A. Dilmanian, …, H. M. Smilowitz. 2010. Gold nanoparticles enhance the radiation therapy of a murine squamous cell carcinoma. *Phys. Med. Biol.* 55:3045–3059.
9. Hainfeld, J. F., H. M. Smilowitz, …, D. N. Slatkin. 2013. Gold nanoparticle imaging and radiotherapy of brain tumors in mice. *Nanomedicine (Lond.).* 8:1601–1609.
10. Chithrani, B. D., A. A. Ghazani, and W. C. Chan. 2006. Determining the size and shape dependence of gold nanoparticle uptake into mammalian cells. *Nano Lett.* 6:662–668.
11. Chithrani, D. B. 2010. Intracellular uptake, transport, and processing of gold nanostructures. *Mol. Membr. Biol.* 27:299–311.
12. Chithrani, D. B., S. Jelveh, …, D. A. Jaffray. 2010. Gold nanoparticles as radiation sensitizers in cancer therapy. *Radiat. Res.* 173:719–728.
13. Cho, S. H. 2005. Estimation of tumour dose enhancement due to gold nanoparticles during typical radiation treatments: a preliminary Monte Carlo study. *Phys. Med. Biol.* 50:N163–N173.
14. Chithrani, D. B. 2010. Nanoparticles for improved therapeutics and imaging in cancer therapy. *Recent Pat. Nanotechnol.* 4:171–180.
15. Chithrani, B. D., and W. C. Chan. 2007. Elucidating the mechanism of cellular uptake and removal of protein-coated gold nanoparticles of different sizes and shapes. *Nano Lett.* 7:1542–1550.
16. Burger, N., A. Biswas, …, M. R. Veldwijk. 2014. A method for the efficient cellular uptake and retention of small modified gold nanoparticles for the radiosensitization of cells. *Nanomedicine (Lond.).* 10:1365–1373.
17. Cremer, C., R. Kaufmann, …, M. Hausmann. 2011. Superresolution imaging of biological nanostructures by spectral precision distance microscopy. *Biotechnol. J.* 6:1037–1051.
18. He, H., C. Xie, and J. Ren. 2008. Nonbleaching fluorescence of gold nanoparticles and its applications in cancer cell imaging. *Anal. Chem.* 80:5951–5957.
19. Yguerabide, J., and E. E. Yguerabide. 1998. Light-scattering submicroscopic particles as highly fluorescent analogs and their use as tracer labels in clinical and biological applications. *Anal. Biochem.* 262: 157–176.
20. Hainfeld, J. F., M. J. O'Connor, …, H. M. Smilowitz. 2014. Infrared-transparent gold nanoparticles converted by tumors to infrared absorbers cure tumors in mice by photothermal therapy. *PLoS One.* 9:e88414.
21. Chris, D., C. D. Geddes, …, J. R. Lakowicz. 2003. Luminescent blinking of gold nanoparticles. *Chem. Phys. Lett.* 380:269–272.
22. Lemmer, P., M. Gunkel, …, C. Cremer. 2008. SPDM—light microscopy with single molecule resolution at the nanoscale. *Appl. Phys. B.* 93:1–12.
23. Lemmer, P., M. Gunkel, …, C. Cremer. 2009. Using conventional fluorescent markers for far-field fluorescence localization nanoscopy allows resolution in the 10-nm range. *J. Microsc.* 235:163–171.
24. Kaufmann, R., P. Lemmer, …, C. Cremer. 2009. SPDM—single molecule superresolution of cellular nanostructures. *Proc. SPIE.* 7185:71850J-19.
25. Grüll, F., M. Kirchgessner, …, U. Kebschull. 2011. Accelerating image analysis for localization microscopy with FPGAs. *In* Proceedings of the 21st International Conference on Field Programmable Logic and Applications. 1–5. doi:http://dx.doi.org/10.1109/FPL.2011.11.
26. Müller, P., Y. Weiland, …, M. Hausmann. 2012. Analysis of fluorescent nanostructures in biological systems by means of spectral position determination microscopy (SPDM). *In* Current Microscopy Contributions to Advances in Science and Technology, *Vol. 1.* A. Méndez-Vilas, editor. FORMATEX Research Center, Badajoz, Spain, pp. 3–12. *http://www.formatex.org/microscopy5/.*
27. Stuhlmüller, M., J. Schwarz-Finsterle, …, G. Hildenbrand. 2015. In situ optical sequencing and structure analysis of a trinucleotide repeat genome region by localization microscopy after specific COMBO-FISH nano-probing. *Nanoscale.* 7:17938–17946.
28. Gossett, W. S. 1908. The probable error of a mean. *Biometrika.* 6:1–25.
29. Kaufmann, R., P. Müller, …, C. Cremer. 2011. Imaging label-free intracellular structures by localisation microscopy. *Micron.* 42:348–352.
30. Jain, P. K., X. Huang, …, M. A. El-Sayed. 2007. Review of some interesting surface plasmon resonance-enhanced properties of noble metal nanoparticles and their applications to biosystems. *Plasmonics.* 2:107–118.